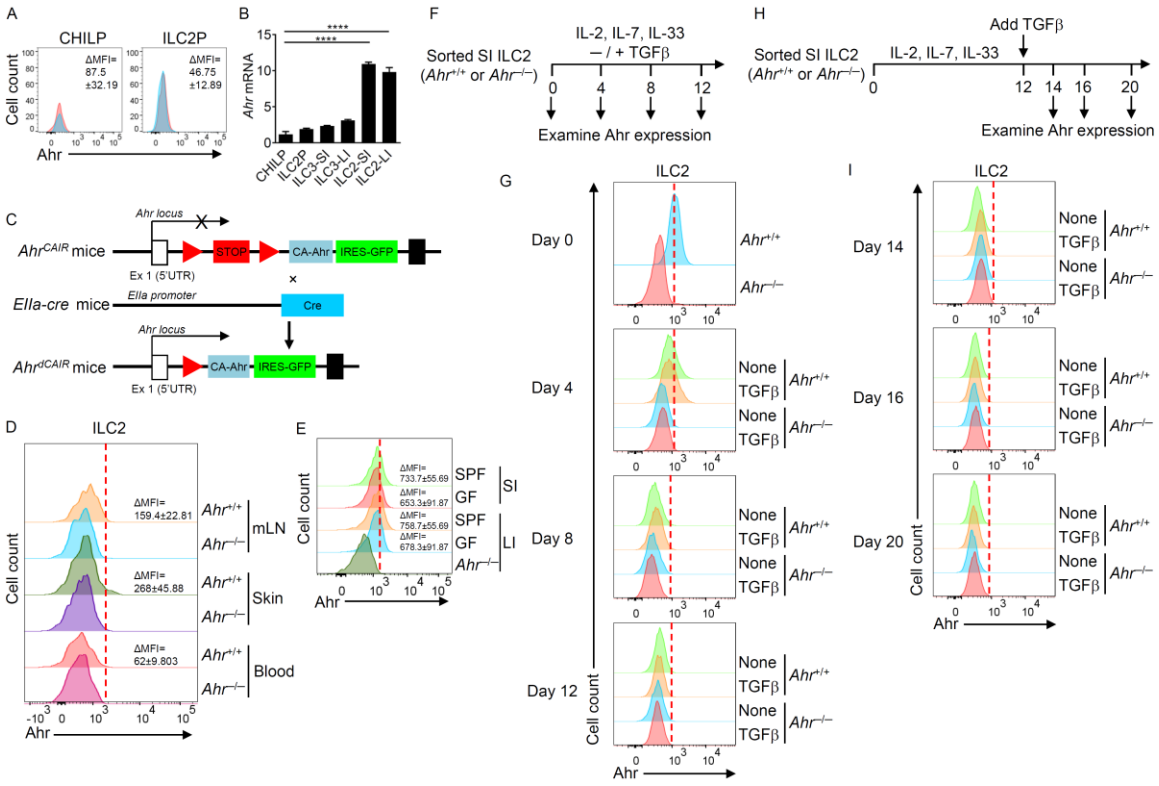

Supplemental Figure 1. Ahr expression in ILC progenitors and mature ILCs, and the effect of TGFβ on Ahr expression, (Related to Figure 1). (A) FACS analysis of Ahr expression in CHILP ($Lin^{-}CD127^{+}\alpha4\beta7^{+}CD25^{-}Flt3^{-}$), and ILC2P ($Lin^{-}CD127^{+}\alpha4\beta7^{+}CD25^{+}Flt3^{-}$) from the bone marrow of $Ahr^{-/-}$or $Ahr^{+/+}$ littermate mice. ΔMFI (Mean Fluorescence Intensity) was calculated as follows: MFI of indicated $Ahr^{+/+}$ cell populations – MFI of indicated $Ahr^{-/-}$ cell populations. Data are representative of three independent experiments. (B) CHILP, ILC2P, ILC2s ($Lin^{-}KLRG1^{+}CD90^{+}$), and ILC3s ($Lin^{-}CD45^{low}CD90^{+}$) were sorted from wildtype C57/BL6 mice. *Ahr* mRNA was analyzed by realtime RT-PCR. Data are shown as mean ± SEM (n=3). ANOVA followed by Bonferroni's test for ILC2s in the small intestine (SI) or large intestine (LI) versus other subsets. ****p<0.0001. (C) Representation of the knock-in mouse model of Ahr^{CAIR} mice with Cre-controlled expression of AhrΔPAS-B (CA-Ahr) and the generation of Ahr^{dCAIR} mice by

crossing *Ahr*$^{CAIR/+}$ mice with *EIIa-cre* mice to delete the loxP-flanked STOP sequence in the germline, and subsequent removal of the *EIIa-cre* transgene by breeding. (D) FACS analysis of Ahr expression in ILC2s from indicated organs. Data are shown as mean ± SEM (n=5 per group). ΔMFI was calculated as follows: MFI of indicated *Ahr*$^{+/+}$ ILC2 populations – MFI of corresponding *Ahr*$^{-/-}$ ILC2s from the same source. (E) FACS analysis of Ahr expression in SI or LI ILC2s (Lin^{-}GATA3^{+}) of specific pathogen free (SPF) or germ-free (GF) mice. Data are shown as mean ± SEM (n=3 per group). ΔMFI was calculated as follows: MFI of indicated ILC2 populations – MFI of *Ahr*$^{-/-}$ SPF LI ILC2s. (F and G) SI ILC2s were sorted from *Ahr*$^{+/+}$ or *Ahr*$^{-/-}$ littermate mice. The cells were then cultured in presence of IL-2, IL-7 and IL-33 (10 ng/ml each), with or without TGFβ (10 ng/ml). ILC2s were collected at indicated time points and intracellular Ahr was determined. Schematic depiction of the experiment (F). FACS analysis of Ahr in *Ahr*$^{+/+}$ or *Ahr*$^{-/-}$ ILC2s from indicated time points (G). (H and I) Sorted SI ILC2s were cultured in presence of IL-2, IL-7 and IL-33 (10 ng/ml each) for 12 days. TGFβ (10 ng/ml) was added on day 12, and ILC2s were harvested at indicated time points. Schematic depiction of the experiment (H). FACS analysis of Ahr in *Ahr*$^{+/+}$ or *Ahr*$^{-/-}$ ILC2s from indicated time points (I).

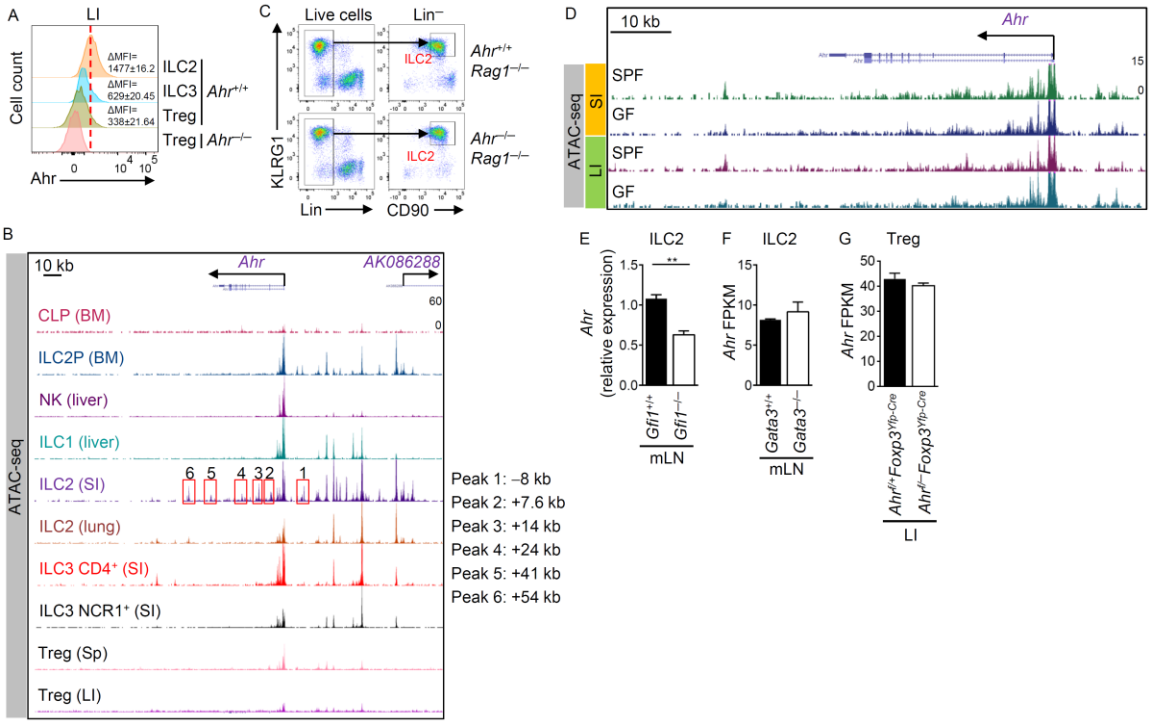

Supplemental Figure 2. Chromatin accessibility at the *Ahr* locus in ILC progenitors, mature ILCs, and Treg cells, (Related to Figure 1). (A) Intracellular staining of Ahr in ILC2s ($Lin^-GATA3^+ROR\gamma t^-$), ILC3s ($Lin^-ROR\gamma t^+GATA3^-$), and Treg cells ($Lin^+Foxp3^+$) isolated from the lamina propria of large intestine (LI). Data are shown as mean ± SEM (n=5 per group). ΔMFI was calculated as follows: MFI of indicated populations – MFI of corresponding population from $Ahr^{-/-}$ mice. (B) Representative ATAC-seq signals at the *Ahr* locus in indicated cell populations. Analysis is based on published ATAC-seq data (Shih et al., 2016; Ye et al., 2017). Red boxes highlight the gut ILC2-specific peaks with indicated distance downstream or upstream from the transcription start site. (C) Sorting strategy of ILC2s from the gut. (D) Representative ATAC-seq signals at the *Ahr* locus in gut ILC2s ($Lin^-KLRG1^+CD90^+$) of SPF or GF C57/BL6 wildtype mice. (E) Relative Ahr expression in the mesenteric lymph nodes (mLN) of Gfi1-sufficient or deficient ILC2s analyzed from published microarray data (Spooner et al., 2013). (F) Fragments Per Kilobase of transcript per Million mapped reads (FPKM) of

Ahr in RNA-seq with sorted ILC2s from mLN of *Gata3*$^{fl/fl}$*-CreERT2* mice, and treated with or without 4-Hydroxytamoxifen (OHT) (Yagi et al., 2014). (G) FPKM of Ahr in RNA-seq from Treg cells sorted from LI of *Ahr*$^{f/+}$*Foxp3*$^{Yfp\text{-}Cre}$ or *Ahr*$^{f/-}$*Foxp3*$^{Yfp\text{-}Cre}$ littermate mice (Ye et al., 2017)

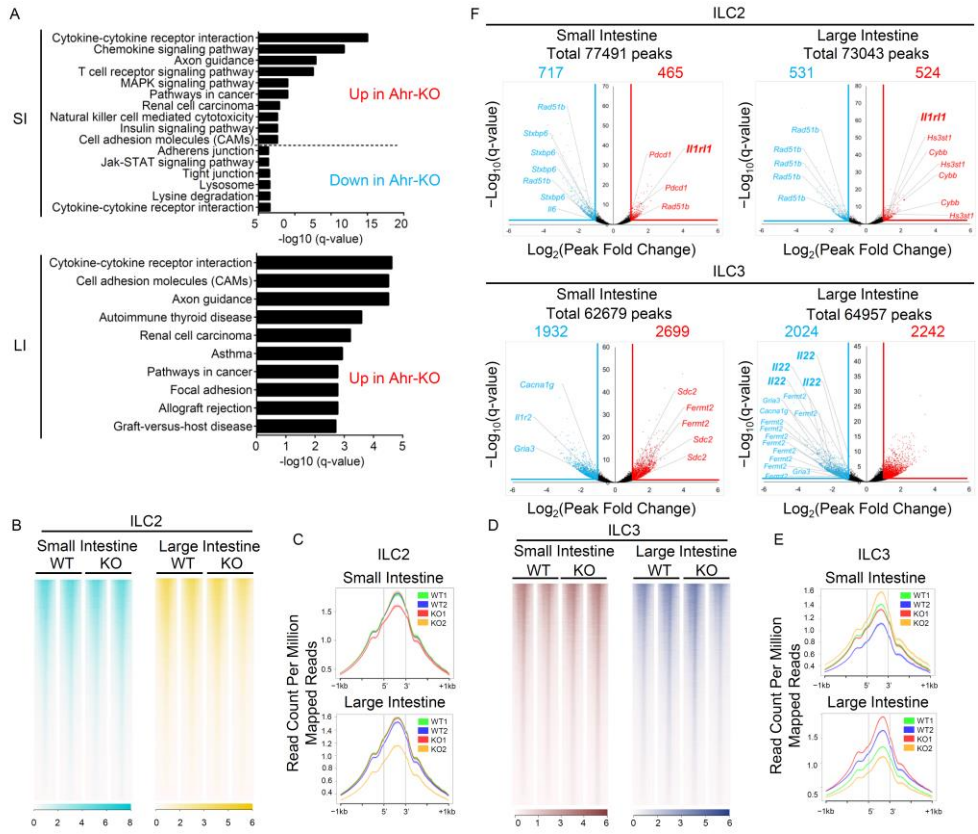

Supplemental Figure 3. Ahr regulates specific gene pathways and chromatin remodeling events in ILCs, (Related to Figure 2). (A) Pathway analysis of differentially-expressed genes identified by RNA-seq in ILC2s (q-value ≤ 0.05) from the small intestine (SI) and large intestine (LI) of *Ahr*$^{+/+}$*Rag1*$^{-/-}$ (WT) or littermate *Ahr*$^{-/-}$*Rag1*$^{-/-}$ (KO) mice. (B, D) ATAC-seq signal across all peak locations comparing ILC2s or ILC3s from SI and LI of *Ahr*$^{+/+}$*Rag1*$^{-/-}$ (WT) or *Ahr*$^{-/-}$ *Rag1*$^{-/-}$ (KO) littermate mice. (C, E) Average ATAC-seq peak signal (Reads Per Million mapped reads; RPM) centered on all peak locations (signal is calculated from 5' to 3' end of the peaks ±1kb) of ILC2s or ILC3s. (F) Volcano plots indicating fold changes between *Ahr*$^{+/+}$*Rag1*$^{-/-}$ (WT) and littermate *Ahr*$^{-/-}$*Rag1*$^{-/-}$ (KO) ILC2s or ILC3s in ATAC-seq signals and q-value. Differentially-expressed peaks (RPM ≥ 1, q-value ≤ 0.05, and fold change ≥ 2) are highlighted in blue (decreased in KO) or red (increased in KO). The differential peaks at the ILC2- or ILC3-characteristic or -associated gene loci were annotated.

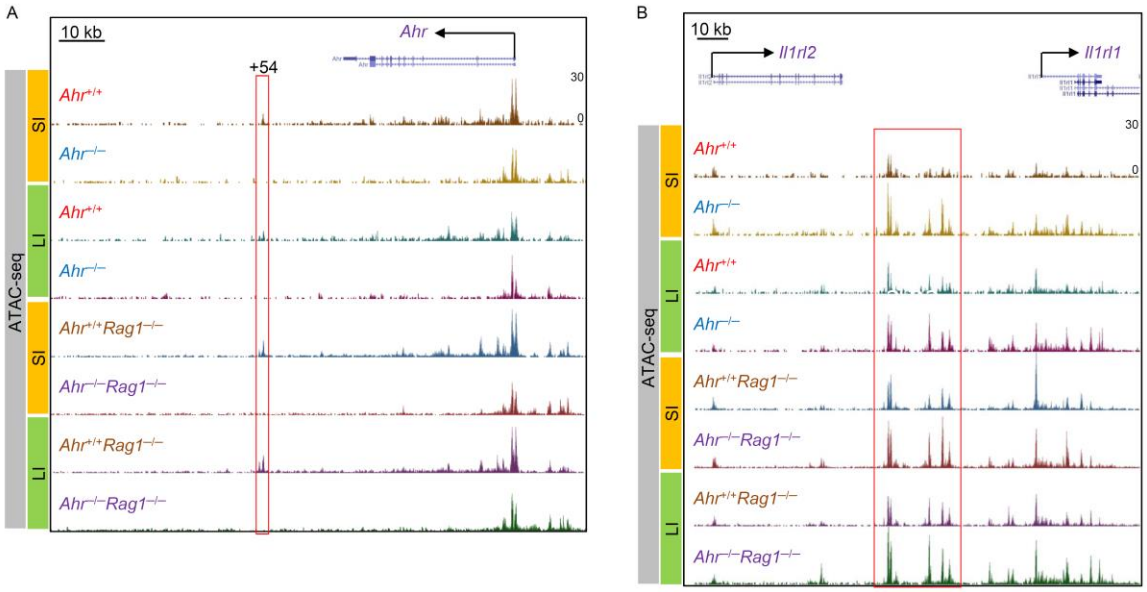

Supplemental Figure 4. The regulation of chromatin at the *Ahr* and *Il1rl1* loci by Ahr is independent of adaptive immunity, (Related to Figure 2). Representative ATAC-seq tracks at the *Ahr* (A) and *Il1rl1* (B) loci in ILC2s sorted from the small intestine (SI) or large intestine (LI) of $Ahr^{+/+}$ or $Ahr^{-/-}$ littermate mice, or $Ahr^{+/+}Rag1^{-/-}$ or $Ahr^{-/-}Rag1^{-/-}$ littermate mice.

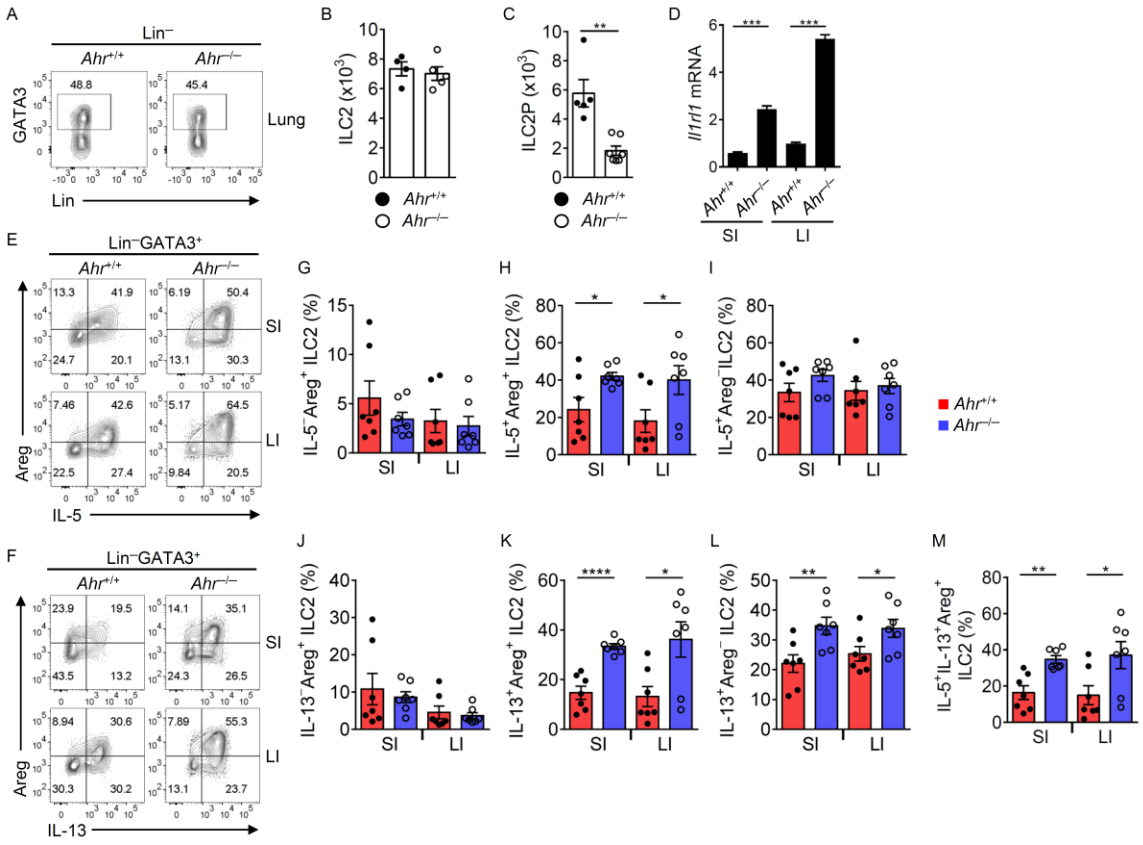

Supplemental Figure 5. Enhanced ST2, IL-5, IL-13, and Amphiregulin expression in Ahr-deficient ILC2s, (Related to Figure 3). (A) FACS analysis of GATA3 expression after gating on Lin$^-$ cells in the lung of *Ahr*$^{+/+}$ or *Ahr*$^{-/-}$ littermate mice. Data are representative of two independent experiments. (B) Absolute numbers of ILC2s (Lin$^-$GATA3$^+$) in the lung of *Ahr*$^{+/+}$ or *Ahr*$^{-/-}$ littermate mice. Data are shown as mean ± SEM (n=4-5 per group). (C) Absolute numbers of ILC2P (Lin$^-$CD127$^+$α4β7$^+$CD25$^+$Flt3$^-$) in the bone marrow of *Ahr*$^{+/+}$ or *Ahr*$^{-/-}$ littermate mice. Data are shown as mean ± SEM (n=5-7 per group). (D) mRNA of ST2 (*Il1rl1*) was determined by realtime RT-PCR. Data are shown as mean ± SEM (n=3). (E to M) FACS analyses of IL-5 and amphiregulin (Areg) expression (E), and IL-13 and Areg expression (F) after gating on Lin$^-$ GATA3$^+$ lamina propria lymphocytes (LPLs) in the small intestine (SI) and large intestine (LI) of *Ahr*$^{+/+}$ or *Ahr*$^{-/-}$ littermate mice. Data are representative of three independent experiments. (G to

M) Percentages of indicated subsets in ILC2s ($Lin^{-}GATA3^{+}$) in SI and LI of $Ahr^{+/+}$ or $Ahr^{-/-}$ littermate mice. Data are shown as mean ± SEM (n=7 per group).

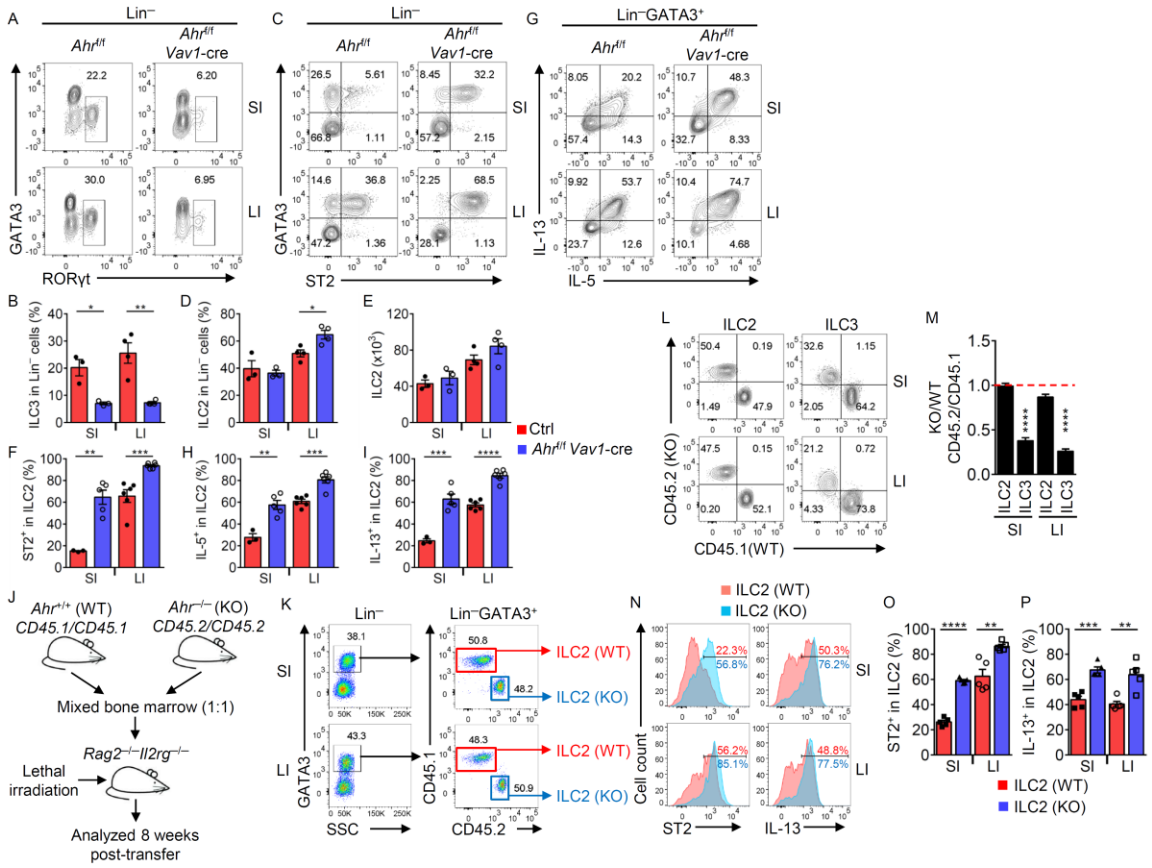

Supplemental Figure 6. Hematopoietic cell-intrinsic regulation of ILC2s by Ahr, (Related to Figure 4). (A to I) FACS analyses of RORγt and GATA3 (A), ST2 and GATA3 expression (C) after gating on Lin$^-$ cells, and IL-5 and IL-13 expression after gating on Lin$^-$GATA3$^+$ cells (G) in the small intestine (SI) and large intestine (LI) of *Ahr$^{f/f}$* and *Ahr$^{f/f}$ Vav-cre* littermate mice. Data are representative of three independent experiments. Percentages of ILC3s (Lin$^-$RORγt$^+$) (B), ILC2s (Lin$^-$GATA3$^+$) (D) among Lin$^-$ cells, and ST2$^+$ cells in ILC2s (F) in SI and LI of Ctrl (*Ahr$^{f/f}$* or *Ahr$^{f/+}$*) and *Ahr$^{f/f}$ Vav-cre* littermate mice. Absolute numbers of ILC2s (E). Data are shown as mean ± SEM (n=3-6 per group). Percentages of IL-5$^+$ (H), and IL-13$^+$ (I) cells in ILC2s (Lin$^-$GATA3$^+$) in SI and LI of Ctrl (*Ahr$^{f/f}$* or *Ahr$^{f/+}$*) and *Ahr$^{f/f}$ Vav1-cre* littermate mice. Data are shown as mean ± SEM (n=3-6 per group). (J to P) Bone marrow from *Ahr$^{+/+}$* (WT, CD45.1/CD45.1) or *Ahr$^{-/-}$* (KO, CD45.2/CD45.2) age and sex matched mice were mixed at equal

ratio, and transferred into lethally irradiated *Rag2*$^{-/-}$*Il2rg*$^{-/-}$ littermate recipient mice. Experimental design of competitive bone marrow chimera (J), and FACS analyses of SSC and GATA3 after gating on Lin$^-$ cells, and CD45.2 and CD45.1 expression by bone marrow-derived ILC2s (Lin$^-$GATA3$^+$) in the small intestine (SI) or large intestine (LI) of recipient mice (K). (L) FACS analysis of CD45.1 and CD45.2 expression by bone marrow-derived ILC2s (Lin$^-$ GATA3$^+$), and ILC3s (Lin$^-$RORγt$^+$) in SI and LI of recipient bone marrow chimeric mice. (M) Ratio of KO (*Ahr*$^{-/-}$) (CD45.2/CD45.2) and WT (*Ahr*$^{+/+}$) (CD45.1/CD45.1) bone marrow-derived ILC2s and ILC3s in competitive bone marrow chimera. Data are shown as mean ± SEM (n=5 per group). Dotted line indicates ratio 1. (N) FACS analysis of ST2 or IL-13 expression by ILC2s (Lin$^-$GATA3$^+$) derived from the bone marrow of *Ahr*$^{+/+}$ (WT) or *Ahr*$^{-/-}$ (KO). Data are representative of five recipient mice. Percentages of ST2$^+$ (O) and IL-13$^+$ (P) cells in the indicated ILC2s. Data are shown as mean ± SEM (n=5 per group).

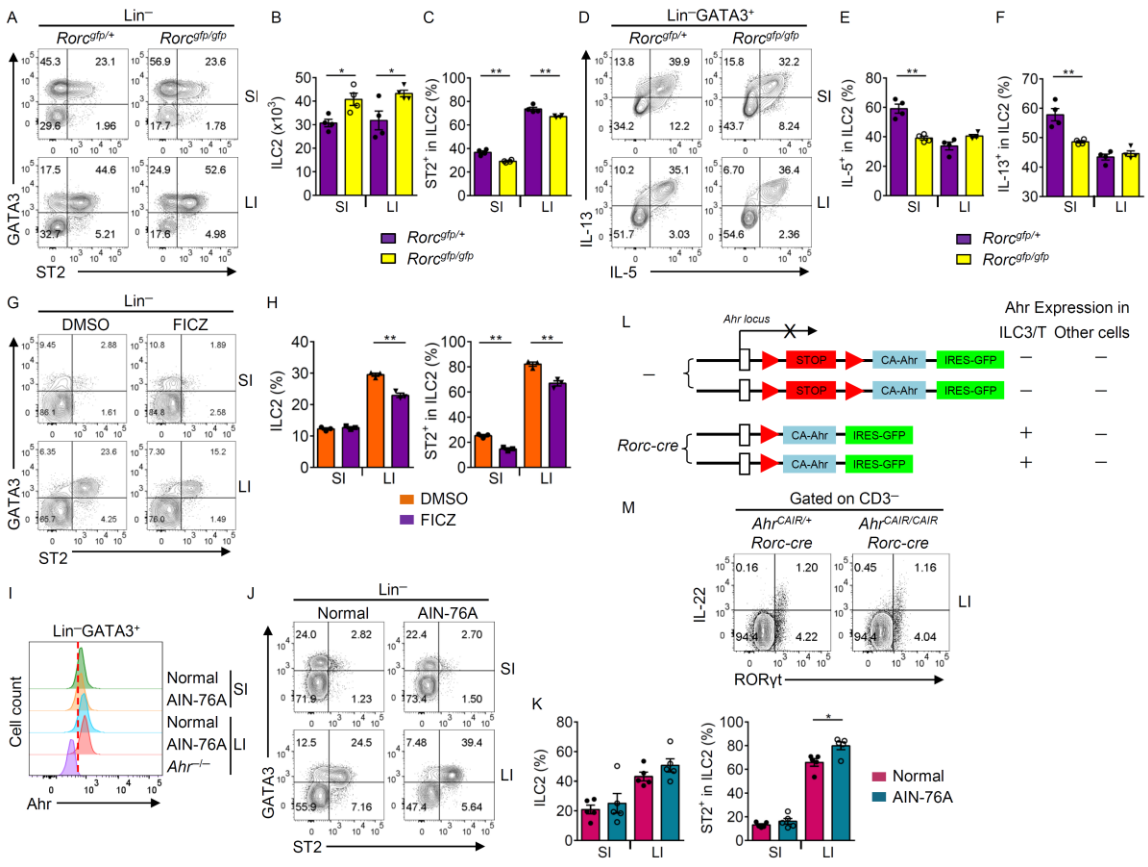

Supplemental Figure 7. Impact of ILC3s deficiency on ILC2s, and regulation of ILCs by ligand or genetic modulation of Ahr activity, (Related to Figures 4 and 7). (A to F) FACS analyses of ST2 and GATA3 after gating on Lin$^-$ lamina propria lymphocytes (LPLs) (A), and IL-5 and IL-13 expression after gating on Lin$^-$GATA3$^+$ LPLs (D) in the small intestine (SI) and large intestine (LI) of *Rorc*$^{gfp/+}$ or *Rorc*$^{gfp/gfp}$ littermate mice. Data are representative of two independent experiments. Absolute number of ILC2s (B), and percentages of ST2$^+$ (C), IL-5$^+$ (E), and IL-13$^+$ (F) cells in ILC2s (Lin$^-$GATA3$^+$) in SI and LI of *Rorc*$^{gfp/+}$ or *Rorc*$^{gfp/gfp}$ littermate mice. Data are shown as mean ± SEM (n=4 per group). (G and H) FACS analysis of ST2 and GATA3 expression after gating on Lin$^-$ lamina propria lymphocytes (LPLs) of littermate wildtype 6 day-old mice treated with FICZ (0.5 μg/day) or vehicle DMSO for 7 days (G). Data are representative of two independent experiments. (H) Percentages of ILC2s (Lin$^-$GATA3$^+$) in

Lin^- LPLs, and $ST2^+$ cells in ILC2s (Lin^-GATA3^+) in the small intestine (SI) and large intestine (LI). Data are shown as mean ± SEM (n=4 per group). FACS analyses of Ahr expression after gating on Lin^-GATA3^+ cells (I), and ST2 and GATA3 expression after gating on Lin^- LPLs (J) of littermate wildtype mice fed with Ahr ligand-deficient diet (AIN-76A) (see STAR Methods). Data are representative of two independent experiments. (K) Percentages of ILC2s (Lin^-GATA3^+) in Lin^- LPLs, and $ST2^+$ cells in ILC2s (Lin^-GATA3^+) in SI and LI. Data are shown as mean ± SEM (n=5 per group). (L) Schematic depiction of generation of *Ahr*$^{CAIR/CAIR}$ *Rorc-cre* mice and Ahr expression in indicated cell populations. (M) FACS analysis of IL-22 and RORγt expression gated on $CD3^-$ LI LPLs of indicated littermate mice. Data are representative of two independent experiments.

Table S1. Primers for realtime RT-PCR and ChIP assays, (Related to STAR Methods)

Actin FW	CTTCTTTGCAGCTCCTTCGTT
Actin RV	AGGAGTCCTTCTGACCCATTC
Ahr FW	GGCTTTCAGCAGTCTGATGTC
Ahr RV	CATGAAAGAAGCGTTCTCTGG
Il1rl1 FW	TGACGGCCACCAGATCATTCACAG
Il1rl1 RV	GCCAAAGCAAGCTGAACAGGCAATAC
Gfi1 FW	AGCGTCGGAGAAGTCACTGT
Gfi1 RV	CAGGTCAGACCCAGCAAGAC
Relmb FW	TGGTGGATCAAAGGATCAAG
Relmb RV	CCACAAGCACATCCAGTGAC
ChIP *Ahr*+54kb FW	CCTCCAGTGACACGCAAGTA
ChIP *Ahr*+54kb RV	CCATCCAGTCTCCACCAGTT
ChIP *Ahr*+14kb FW	CCTTGACCCAACAAGAGTGAA
ChIP *Ahr*+14kb RV	TGGAGTCAGCAGTTGACAGG
ChIP *Il1rl1*-11kb FW	ACTTATCTAACCCTCCTCACCC
ChIP *Il1rl1*-11kb RV	AAGTAGCAGCCTGTCTGAACTAC
ChIP *Il1rl1*-2kb FW	AGGGTAGAGTCATAGGCCAAC
ChIP *Il1rl1*-2kb RV	TGTGATAGTCTTTCCTCGTGAGC